10.1098/rspa.2001.0882

THE ROYAL SOCIETY

Surface scattering in three dimensions: an accelerated high-order solver

By Oscar P. Bruno and Leonid A. Kunyansky†

Applied Mathematics, California Institute of Technology, 1200 E California Boulevard, Pasadena, CA 91125, USA

Received 2 June 2000; revised 19 August 2000; accepted 16 July 2001

We present a new algorithm for the numerical solution of problems of acoustic scattering by surfaces in three-dimensional space. This algorithm evaluates scattered fields through fast, high-order, accurate solution of the corresponding boundary integral equation. The high-order accuracy of our solver is achieved through use of *partitions of unity* together with *analytical* resolution of kernel singularities. The acceleration, in turn, results from use of high-order *equivalent source* approximations, which allow for fast evaluation of non-adjacent interactions by means of the three-dimensional fast Fourier transform (FFT). Our acceleration scheme has dramatically lower memory requirements and yields much higher accuracy than existing FFT-accelerated techniques. The present algorithm computes one matrix-vector multiply in $\mathcal{O}(N^{6/5}\log N)$ to $\mathcal{O}(N^{4/3}\log N)$ operations (depending on the geometric characteristics of the scattering surface), it exhibits super-algebraic convergence, and it does not suffer from accuracy breakdowns of any kind. We demonstrate the efficiency of our method through a variety of examples. In particular, we show that the present algorithm can evaluate accurately, on a personal computer, scattering from bodies of acoustical sizes (ka) of several hundreds.

Keywords: wave scattering; integral equation; fast algorithm; fast Fourier transform; equivalent sources; spherical wave expansion

1. Introduction

The calculation of wave scattering from surfaces of acoustically or electrically large objects remains one of the most important and challenging problems in computational science. Roughly, these problems present difficulties as they require accurate descriptions and manipulation of highly oscillatory functions. Scattering problems involving one-dimensional integrals have been efficiently treated by means of high-order integrators (including the exponentially accurate trapezoidal rule and other high-order schemes (Colton & Kress 1992; Rokhlin 1990)), which reduce dramatically the complexity necessary to meet a given accuracy requirement. Problems of scattering by surfaces in three-dimensional space are much more complex, however.

A number of fast algorithms for three-dimensional scattering have been introduced in the last two decades (Bleszynski *et al.* 1996; Bojarski 1982; Catedra *et al.* 1989; Coifman *et al.* 1993; Phillips & White 1997; Rokhlin 1993; Song *et al.*

† Present address: Department of Mathematics. University of Arizona, Tucson, AZ 85721, USA.

1988, 1997). These methods are considerably faster than classical non-accelerated algorithms—they run in $\mathcal{O}(N \log N)$ to $\mathcal{O}(N^{3/2} \log N)$ operations (where N is the number of discretization points) in contrast with the $\mathcal{O}(N^2)$ operations required by non-accelerated schemes—and thus they allow for computations involving rather large scattering surfaces. None of the existing fast implementations exhibits high-order convergence, however. As a result, the error of such fast computations turns out to be of the order of a fraction of a decibel (or several per cent) even for the simplest test scatterers (Canino *et al.* 1998; Song *et al.* 1988). In this paper we present an $\mathcal{O}(N^{6/5} \log N)$ to $\mathcal{O}(N^{4/3} \log N)$ algorithm which, through a novel combination of numerical techniques, allows for fast and *high-order accurate* solution of problems of acoustic scattering. (The latter estimate applies to smooth surfaces, for which our high-order algorithm provides accurate solutions with small values of N; the former, more favourable count is valid for highly complex surfaces requiring significant amounts of subwavelength sampling.) This algorithm exhibits super-algebraic convergence, it requires limited amounts of RAM, and it does not suffer from accuracy breakdowns of any kind. We demonstrate the efficiency of our methods through a variety of numerical examples—including very accurate evaluation on small personal computers of scattering from bodies of acoustical sizes (ka) of several hundreds.

The algorithm we present consists of two main elements: a basic high-order local integrator and a high-order acceleration scheme. Our basic high-order integrator involves use of partitions of unity—to deal with topological characteristics of closed surfaces—and analytical resolution of kernel singularities—to avoid costly refinement strategies. Use of this algorithm without acceleration would lead to the customary $O(N^2)$ operation count. The constant of proportionality in this complexity estimate is rather small, however, so that, even without acceleration, the high-order integrator is an efficient solver for small to medium-sized problems. For large problems, however, use of acceleration is imperative.

Two well-known approaches to acceleration have been available for a number of years: the fast multipole method (FMM) (Coifman *et al.* 1993; Rokhlin 1990, 1993; Song *et al.* 1988, 1997) on the one hand, and a broad class of fast Fourier transform (FFT) accelerated techniques and k-space methods (Bleszynski *et al.* 1996; Bojarski 1982; Catedra *et al.* 1989; Phillips & White 1997) on the other. FMM-based algorithms provide considerable acceleration: they run in as little as $\mathcal{O}(N \log N)$ operations per iteration. However, to the best of our knowledge, high-order accuracy has not been demonstrated in FMM computations of wave scattering. A possible explanation for this fact is that the FMM approach (Coifman *et al.* 1993; Rokhlin 1993) depends critically on certain mappings which contain multiplication by Hankel functions of high order. These operations are associated with a substantial amount of ill conditioning, which leads to accuracy limitations known as the 'subwavelength breakdown problem' (see Dembart & Yip 1998, p. 51; Labreuche 1998, p. 576; Greengard *et al.* 1998). These limitations may prevail and mask the asymptotic high-order convergence of any underlying high-order integrator, however accurate. In contrast, the FFT acceleration techniques are stable.

The accelerator we introduce is closely related to two of the most advanced FFT methods developed recently (Bleszynski *et al.* 1996; Phillips & White 1997). An important common element between these two methods and our technique is the concept of equivalent (or auxiliary) sources, located on a subset of a three-dimensional Cartesian grid. In all three cases, the intensities of these sources are chosen to approx-

imate the field radiated by the scatterer, which allows for a fast computation of numerous non-adjacent interactions through the use of the three-dimensional FFT. In Bleszynski *et al.* (1996) and Phillips & White (1997), both volumetric and surface scattering problems are treated; our present discussion, in contrast, only applies to surface scattering problems. Surface problems are treated in Bleszynski *et al.* (1996) and Phillips & White (1997) by means of equivalent sources located in a volumetric grid—in such a way that equivalent sources with non-zero intensities occupy *all Cartesian nodes adjacent to the surface*. Since the spacing of this Cartesian grid cannot be coarsened beyond some threshold, and, further, since the three-dimensional convolution should be performed throughout the whole volume occupied by the body, such a scheme requires a $\mathcal{O}(N^{3/2})$ FFT. Therefore, the traditional FFT surface scattering solvers require $\mathcal{O}(N^{3/2})$ units of RAM and run in $\mathcal{O}(N^{3/2}\log N)$ operations.

Our algorithm, in contrast, subdivides the volume occupied by the scatterer into a number of (relatively large) cubic cells, and it places equivalent sources *on the faces* of those cells. Such a design reduces significantly the sizes of the required FFTs, to $\mathcal{O}(N^{6/5})$–$\mathcal{O}(N^{4/3})$ points, with proportional improvement in storage requirements and operation count. Further, it results in super-algebraic convergence of the equivalent source approximations *as the size of the scatterer is increased*. In view of its high-order character and its improved acceleration technique, the present algorithm can evaluate solutions to large scattering problems in short computing times, very accurately and with very small memory requirements; see § 6.

2. Mathematical formulation

We consider a problem of acoustic scattering by a sound-soft obstacle. This problem, which is governed by the Helmholtz equation, can be treated using the acoustic single- and double-layer potentials (Colton & Kress 1992):

$$(S\varphi)(\boldsymbol{r}) = \int_{\partial D} \Phi(\boldsymbol{r}', \boldsymbol{r})\varphi(\boldsymbol{r}')\,\mathrm{d}s(\boldsymbol{r}') \quad \text{and} \quad (K\varphi)(\boldsymbol{r}) = \int_{\partial D} \frac{\partial \Phi(\boldsymbol{r}', \boldsymbol{r})}{\partial \boldsymbol{\nu}(\boldsymbol{r}')}\varphi(\boldsymbol{r}')\,\mathrm{d}s(\boldsymbol{r}'). \tag{2.1}$$

Here $\Phi(\boldsymbol{r}', \boldsymbol{r}) = \mathrm{e}^{\mathrm{i}k|\boldsymbol{r}'-\boldsymbol{r}|}/4\pi|\boldsymbol{r}'-\boldsymbol{r}|$ is the Green function for the Helmholtz equation, and $\boldsymbol{\nu}(\boldsymbol{r})$ is the external normal to the surface ∂D at point $\boldsymbol{r}$. Explicitly, given the values of the incoming wave $\psi^i(\boldsymbol{r})$ on ∂D, the scattered field can be found easily once the integral equation for the unknown density $\varphi(\boldsymbol{r})$,

$$\tfrac{1}{2}\varphi(\boldsymbol{r}) + (K\varphi)(\boldsymbol{r}) - \mathrm{i}\gamma(S\varphi)(\boldsymbol{r}) = \psi^i(\boldsymbol{r}), \qquad \boldsymbol{r} \in \partial D, \tag{2.2}$$

has been solved. (Here γ is an arbitrary positive constant; appropriate choices of this parameter can be very advantageous in practice—see § 5 *c*.) Naturally, the possibility of producing fast and accurate solutions for our problems hinges on our ability to evaluate the integrals (2.1) accurately and efficiently. In attempting to develop such accurate and efficient integrators one faces two main problems, namely, accurate evaluation of the singular *adjacent interactions*—without undue compromise of speed—and fast evaluation of the voluminous number of *non-adjacent interactions*—without compromise in accuracy.

Our approach to a solution of these problems is described in what follows. Section 3 introduces the partitions of unity we use to deal with the topological characteristics of closed surfaces. The basic high-order integrator is presented in § 4. In § 5 we describe

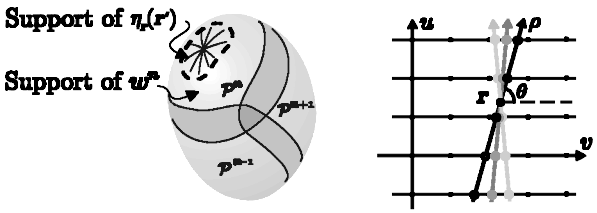

(*a*) (*b*)

Figure 1. (*a*) POU covering and region of singular integration. (*b*) Integration in a polar system; empty circles indicate discretization points for the integration with respect to ρ.

our acceleration scheme. Finally, a variety of numerical examples and comparison with other work are provided in § 6. Proofs and numerical illustrations of convergence and stability of our methods are presented in Kunyansky & Bruno (2001).

3. Partitions of unity, discretizations

In order to deal with topological characteristics of closed surfaces and the singular character of integrands, we use a patching strategy based on use of both *fixed* and *floating* partitions of unity (POU), which we define in what follows.

Fixed POU are used to deal with surfaces which, possibly, can only be parametrized locally. In detail, we begin by considering a covering of the surface ∂D by a number K of overlapping two-dimensional patches $\mathcal{P}^j$, $j = 1, \ldots, K$, each one of which is smoothly mapped to coordinate sets $\mathcal{H}^j$ in two-dimensional space, where actual integrations are performed. Further, we use a POU subordinated to this covering of ∂D, i.e. a set of non-negative smooth functions $\{w^j, j = 1, \ldots, K\}$, such that (i) w^j is defined, smooth and non-negative in ∂D, and it vanishes outside $\mathcal{P}^j$, and (ii) $\sum_{j=1}^{K} w^j = 1$ throughout ∂D. This POU, which we refer to as the fixed POU, allows us to reduce the problem of integration of the density $\varphi(\boldsymbol{r}')$ over the surface to a calculation of integrals involving products of kernels with certain smooth densities φ^j *over square domains* $\mathcal{Q}^j$—via a trivial extension of the φ^j by zero.

The (Nyström) discretization of our problem is introduced through the patch-parametrizations mentioned above. In detail, the unknown density we seek is characterized by its values on the nodes of Cartesian grids on the integration domains $\mathcal{Q}^j$. As shown in the rest of this section and § 4, use of the fixed POU together with these regular Cartesian meshes and certain changes of variables allow us to reduce our singular integration problem to evaluation of integrals of *smooth periodic functions*—which can be computed with spectral accuracy by means of the trapezoidal rule; see also Bruno & Kunyansky (2001*a*).

In addition to the fixed POU we introduce *floating* POU, which help us accelerate the integration method. To motivate the introduction of the floating POU we begin by considering the integration problem (2.1) for one of the densities φ^j at a surface point $\boldsymbol{r}$ outside $\mathcal{P}^j$. Clearly the integrand is smooth for such a target point $\boldsymbol{r}$, so the trapezoidal rule in $\mathcal{Q}^j$ yields the integral with spectral accuracy. The singular integral with $\boldsymbol{r} \in \mathcal{Q}^j$, in turn, can be reduced to smooth integrations by the changes to polar coordinates introduced in § 4. For purposes of acceleration, however, it is necessary to reduce the regions where such coordinate transformations are operative. We thus introduce the *floating POU*: for every point $\boldsymbol{r} \in \mathcal{Q}^j$ the density φ^j is smoothly split in

the form $\varphi^j = \eta_{\boldsymbol{r}}(\boldsymbol{r}')\varphi^j + (1 - \eta_{\boldsymbol{r}}(\boldsymbol{r}'))\varphi^j$; see figure 1*a*. Here $\eta_{\boldsymbol{r}}$ is a smooth function which equals unity in a neighbourhood of $\boldsymbol{r}$ and is compactly supported inside the cube $\mathcal{S}_i$ for which $\boldsymbol{r} \in c_i$; see § 5 for the definitions of $\mathcal{S}_i$ and c_i. Note that, as before, the trapezoidal rule can be used to evaluate the integral containing $(1 - \eta_{\boldsymbol{r}}(\boldsymbol{r}'))\varphi^j$, whereas the methods based on polar changes of coordinates of § 4, in turn, apply effectively to the integral containing the term $\eta_{\boldsymbol{r}}(\boldsymbol{r}')\varphi^j$.

It is not difficult to obtain numerical POU in the present setting: their basic components $W_j(u, v)$ can be constructed in the parameter spaces $\mathcal{H}^j$, $j = 1, \ldots, K$. The functions $W_j(u, v)$ should be smooth and non-negative, and the support of $W_j(u, v)$ should be contained in the open set $\mathcal{H}^j$, so that, in particular, all derivatives of $W_j(u, v)$ vanish on the boundary of $\mathcal{H}^j$. We note that the functions $W_j(u(\boldsymbol{r}), v(\boldsymbol{r}))$ can be extended (as zero) to functions defined globally on ∂D. Thus, selecting W_js so that $\sum_{\ell=1}^{K} W_\ell(u(\boldsymbol{r}), v(\boldsymbol{r}))$ does not vanish anywhere on ∂D we may define a partition of unity by

$$w_j(\boldsymbol{r}) = \frac{W_j(u(\boldsymbol{r}))}{\sum_{\ell=1}^{K} W_\ell(u(\boldsymbol{r}))}.$$

It is easy to construct functions W_j satisfying the conditions above. In our codes we have used products of functions of the type $E(u)E(v)$ and $E(\sqrt{u^2 + v^2})$, where, for real t, $E(t)$ is defined as follows:

$$E(t) = \begin{cases} 1, & \text{for } t \leqslant t_0, \\ \exp\left(\dfrac{2\mathrm{e}^{-1/x}}{x - 1}\right), & \text{for } t_0 < t < t_1, \quad \text{where } x = \dfrac{|t| - t_0}{t_1 - t_0}, \\ 0, & \text{for } t \geqslant t_1. \end{cases}$$

4. Adjacent integration

Substantial difficulties in the high-order evaluation of *adjacent interactions* are caused by the singular nature of the integral kernels $\Phi(\boldsymbol{r}', \boldsymbol{r})$ and $\partial\Phi(\boldsymbol{r}', \boldsymbol{r})/\partial\boldsymbol{\nu}(\boldsymbol{r}')$ at $\boldsymbol{r}' = \boldsymbol{r}$. While, certainly, the well-known strategy of 'singularity subtraction' gives rise to bounded integrands, integration of such bounded functions by means of classical high-order methods does not exhibit high-order accuracy—since the subsequent derivatives of the integrand are themselves unbounded. Thus, specialized quadrature rules must be developed and used to achieve high-order integration.

Our approach to high-order integration is based on analytical resolution of the kernel singularities. The resolution is achieved by integration in polar coordinates centred around each target point $\boldsymbol{r}$ in our Cartesian grid, as indicated in figure 1*b*. The Jacobian of the corresponding change of variables cancels the singularity—and, in fact, it produces integrands which are smooth in any radial direction. Together with the partitions of unity mentioned above, this change of variables reduces the radial integration problem to evaluation of integrals of smooth *periodic* functions: radial periodicity results from the partitions of unity, which make the integrands and all of their derivatives vanish on the boundary of the integration domain. Since the radial integrals are themselves smooth periodic functions of the angular variable, all involved integrals can be evaluated accurately by means of the trapezoidal rule, thus, providing a high-order solution to the complete adjacent integration problem.

The integrands are represented by their values at the nodes of a Cartesian grid, and, thus, an interpolation technique is needed to obtain the necessary function

values on appropriate radial grids. Efficiency is of utmost importance here, since our scheme uses one such polar coordinate transformation *at each target point*. Fortunately, such fast interpolations can be performed with high accuracy by taking advantage of the high-order convergence of trigonometric approximations of periodic functions in conjunction with FFTs. The details of our fast interpolation algorithm are as follows.

1. Using the one-dimensional FFT, construct a set of Fourier series interpolating the values of the densities along coordinate lines of the Cartesian grid. (Interpolations in vertical direction are to be used for integrations corresponding to $\theta \in [-\pi/4, \pi/4]$ while horizontal interpolations should be applied in the complementary set of directions; see figure 1*b*.) Since the densities are smooth and vanish on the patch boundaries, such polynomials yield a high-order approximation to the densities.

2. Refine the grid along coordinate lines. Use one-dimensional FFTs to evaluate the resulting Fourier series (and possibly their derivatives) on the refined grid.

3. Use the function values on the refined grids to construct one or more interpolating polynomials (e.g. Chebyshev, splines, etc.) per original grid interval.

As a result of this procedure one obtains polynomial interpolants that closely approximate the interpolating Fourier series. The use of the FFT makes the interpolation times negligible when compared with those required by the other stages of the algorithm; evaluation of the polynomials at the required points (shown in figure 1*b*), on the other hand, requires few multiplications and additions per point and is therefore also very fast.

(In our numerical examples we used a 16-fold one-dimensional refinements of the original coordinate grids. Further, we used polynomials of degree three such that their values and the values of their first derivatives coincide with those of the corresponding trigonometric polynomial at the endpoints of each subgrid interval. Clearly the convergence of this interpolating algorithm is of fourth order in the subgrid spacing. One could certainly use increasingly larger subgrids and Chebyshev interpolation to produce a interpolation technique of super-algebraic convergence. This is a matter of limited interest in practice, however. Indeed, in the cases we have considered, the cubic interpolation method with a 16-fold refinement described above matches the accuracy of the underlying trigonometric approximation to $\mathcal{O}(10^{-9})$ in computing times of the order of 1% of the time required by the overall computation; see, for example, table 1. These accuracies are higher than those of interest in all of the problems we have treated, so that the use of more sophisticated interpolating techniques does not seem necessary.)

The high-order integrator described in this section exhibits super-algebraic convergence for infinitely smooth scattering surfaces. (Extensions to high-order integrators for non-smooth surfaces are given in Bruno & Kunyansky (2001*b*); see also § 6.) Use of this algorithm without acceleration would lead to the customary $O(N^2)$ operation count. However, since this method resolves singularities analytically, low discretization densities suffice to yield accurate results, and, thus, even without acceleration, our high-order integrator gives rise to an efficient solver for small to medium-sized problems. For large problems acceleration becomes imperative; our acceleration technique is described in the following section.

We conclude this section with a remark on related work: the regularizing effect of changes of variables on singular kernels is known (Duffy 1982). We believe, however, that integration in the polar coordinates in combination with a Nyström discretization scheme have not been used before. Note that, indeed, use of a straightforward high-order Cartesian-to-polar interpolator would lead to inordinate computational times, since such polar change of variables must be performed around *each target point*.

5. Non-adjacent integration and acceleration

We begin by considering a cube C containing the obstacle. (For elongated obstacles a three-dimensional slab is preferable; for simplicity of presentation, however, we will limit our discussion to covering by a cube.) Denoting the acoustical size of the cube by A, we partition the cube C into a number A^2 of smaller equal non-overlapping cubic cells c_i of side $H = A^{1/3}$, so that there are $A^{2/3}$ cells along each edge of the cube. We note that each one of our surface discretization points is contained in one of the cells c_i; many of the cells contain no sources in their interior. As we shall see, it is necessary for our method to use cells c_i which do not admit inner resonances (eigenfunctions of the Dirichlet Laplacian) for the given wavenumber k. This can be insured easily by adjusting slightly the cell size H.

(*a*) *Equivalent sources*

We seek to substitute the surface sources contained in a cubic cell c_i by certain 'equivalent sources' on the faces of c_i, in such a way that the field produced by the true and equivalent sources coincide on non-adjacent portions of the scattering surface, to within a prescribed numerical accuracy. (More precisely, the approximation corresponding to a cell c_i will be valid outside the concentric cube $\mathcal{S}_i$ of side $3H$, with exponentially small errors (see Bruno & Kunyansky 2001*a*; Kunyansky & Bruno 2001). Points outside $\mathcal{S}_i$ will be referred to as non-adjacent to c_i.) As we will see, for computational efficiency it is favourable to use a sequence of three independent sets of equivalent sources, located on three corresponding sets of points Π^ℓ, $\ell = 1, 2, 3$. Here Π^ℓ is a Cartesian grid of points contained in the union of all cell faces parallel to the coordinate plane $x_\ell = 0$.

For each ℓ, equivalent sources (monopoles $\xi^{\mathrm{m}}_\ell \Phi(\boldsymbol{r}_\ell, \boldsymbol{r})$ and dipoles $\xi^{\mathrm{d}}_\ell \partial\Phi(\boldsymbol{r}_\ell, \boldsymbol{r})/\partial x_\ell(\boldsymbol{r}')$ of intensity ξ^{m}_ℓ and ξ^{d}_ℓ, respectively) are to be placed in appropriately chosen subsets Π^ℓ_i of Π^ℓ. In detail, the set Π^ℓ_i consists of all the points in Π^ℓ which lie within the union of two circular domains concentric with (and containing) the faces of c_i in Π^ℓ, as shown in figure 2. The radius of these domains is chosen to be equal to (or slightly larger than) the length of the diagonals of the faces (experimentally it was found that increase of the radius up to 40% leads to somewhat higher accuracy and relatively small increases in computing times). The intensities ξ^{m}_ℓ and ξ^{d}_ℓ of the equivalent sources are then chosen in such a way that the radiated field evaluated at the n^{coll} collocation points on $\partial\mathcal{S}_i$, is equal, within a prescribed tolerance, to the field generated by the true sources located within c_i. As shown in Kunyansky & Bruno (2001) it is indeed necessary to use both monopoles and dipoles to obtain convergent approximations from two-face representations of these types.

The spacing of the Cartesian grid containing equivalent sources is taken to equal $1/k$, so that there are k^2H^2 nodes on each face of a cubic cell. Then, the total number

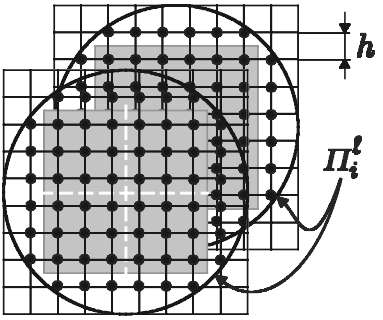

Figure 2. Locations of the equivalent sources (black circles); grey squares indicate faces of a cell c_i

n^{source} of monopoles and dipoles inside the circular domains is greater than or equal to $4k^2H^2$, which makes the acceleration scheme exponentially accurate (Kunyansky & Bruno 2001). For best performance, the number n^{coll} of collocation points is chosen to be no smaller than $2n^{\text{source}}$; see table 2 in Kunyansky & Bruno (2001).

The intensities $\boldsymbol{\xi} = (\xi_\ell^m, \xi_\ell^d)$ can be obtained as a solution of the linear system,

$$\boldsymbol{A}\boldsymbol{\xi} = \boldsymbol{b}, \tag{5.1}$$

where $\boldsymbol{b} = (b_1, b_2, \ldots b_{n^{\text{coll}}})$ is a vector containing values of the field generated on $\partial\mathcal{S}_i$ by the true surface sources, and $\boldsymbol{A}$ is a $(n^{\text{coll}} \times n^{\text{source}})$ matrix. Since the number of equations n^{coll} exceeds the number n^{source} of unknowns this linear system cannot be solved exactly; instead we use the QR decomposition (Golub & Van Loan 1989) to find a least-squares solution $\boldsymbol{\xi}$. Equations (5.1) for the equivalent sources must be solved in each one of the non-empty cells c_i. Since the geometry and meshes in all of the cells are identical, the matrix $\boldsymbol{A}$ is the same for all the c_i. Thus the QR factorization of $\boldsymbol{A}$ needs only to be computed once for each scattering problem.

We note that by placing collocation points on square Cartesian grids on the surface of cube $\mathcal{S}_i$ in an appropriately symmetric fashion one induces certain symmetries in the system (5.1) which can be exploited to transform (5.1) into a block diagonal system containing eight blocks. This transformation gives rise to a (significant) eight-fold reduction in the computational expense required to obtain the intensities $\boldsymbol{\xi}$; see Bruno & Kunyansky (2001*a*).

(*b*) *Evaluation of* $\psi_\ell^{\text{na,eq}}(\boldsymbol{r})$ *for* $\boldsymbol{r}$ *in the three-dimensional grid*

The methods introduced in the previous section allow us to identify the field produced by the portion of the scattering surface contained within a cell c_i with the corresponding field produced by the equivalent sources on Π_i^ℓ *at all points outside* $\mathcal{S}_i$. In other words, recalling the definition of adjacency of § 5 *a*, denoting by $\psi_\ell^{\text{na,eq}}(\boldsymbol{r})$ the field induced at point $\boldsymbol{r}$ by all the equivalent sources non-adjacent to $\boldsymbol{r}$ and calling $\psi_\ell^{\text{a,true}}(\boldsymbol{r})$ the field induced at point $\boldsymbol{r}$ by all adjacent true surface sources, the field ψ induced by all surface sources at any point $\boldsymbol{r}$ in space is given by

$$\psi(\boldsymbol{r}) = \psi_\ell^{\text{na,eq}}(\boldsymbol{r}) + \psi_\ell^{\text{a,true}}(\boldsymbol{r}) + \varepsilon_\ell, \tag{5.2}$$

where $|\varepsilon_\ell| < \varepsilon$, and ε is the prescribed numerical tolerance. In this section we present an efficient algorithm for the evaluation of $\psi_\ell^{\text{na,eq}}(\boldsymbol{r})$ at all points $\boldsymbol{r}$ in the three-dimensional grid.

The acceleration algorithm uses a quantity related to those occurring in equation (5.2), namely, the field $\psi_\ell^*(\boldsymbol{r})$ produced at a grid point $\boldsymbol{r}$ by all of the equivalent sources except the one at point $\boldsymbol{r}$, where the Green's function is infinite. Using the notation,

$$\Phi^*(\boldsymbol{r}-\boldsymbol{r}_\ell)=\begin{cases}\dfrac{\mathrm{e}^{\mathrm{i}k|\boldsymbol{r}-\boldsymbol{r}_\ell|}}{4\pi|\boldsymbol{r}-\boldsymbol{r}_\ell|}, & \text{for } \boldsymbol{r}\neq\boldsymbol{r}_\ell,\\ 0, & \text{for } \boldsymbol{r}=\boldsymbol{r}_\ell,\end{cases}$$

$$\Psi_\ell^*(\boldsymbol{r}-\boldsymbol{r}_\ell)=\begin{cases}\dfrac{\partial}{\partial x_\ell(\boldsymbol{r}')}\dfrac{\mathrm{e}^{\mathrm{i}k|\boldsymbol{r}-\boldsymbol{r}_\ell|}}{4\pi|\boldsymbol{r}-\boldsymbol{r}_\ell|}, & \text{for } \boldsymbol{r}\neq\boldsymbol{r}_\ell,\\ 0, & \text{for } \boldsymbol{r}=\boldsymbol{r}_\ell,\end{cases}$$

we have

$$\psi_\ell^*(\boldsymbol{r})=\sum_{\text{grid sources}}[\xi_\ell^{\mathrm{m}}\cdot\Phi^*(\boldsymbol{r}-\boldsymbol{r}_\ell)+\xi_\ell^{\mathrm{d}}\cdot\Psi_\ell^*(\boldsymbol{r}-\boldsymbol{r}_\ell)]. \tag{5.3}$$

We note that ψ_ℓ^* is not an approximation to any of the physical quantities under consideration since, at any given $\boldsymbol{r}\in\partial D$, the quantity $\psi_\ell^*(\boldsymbol{r})$ contains only poor approximations of contributions from sites adjacent to $\boldsymbol{r}$. Subtraction of these poor approximations would then complete the evaluation of $\psi_\ell^{\mathrm{na,eq}}(\boldsymbol{r})$.

The importance of the quantity ψ_ℓ^* lies, of course, in the fact that, being an exact convolution in a Cartesian grid, it can be evaluated accurately and efficiently by means of the FFT. The required quantity $\psi_\ell^{\mathrm{na,eq}}$ can be obtained from ψ_ℓ^* by subtracting contributions from adjacent cells. Since the equivalent sources are located in the nodes of three-dimensional rectangular grid, the contributions from adjacent cells are given by three-dimensional convolutions, which can be obtained efficiently by means of (small) three-dimensional FFTs. Having obtained $\psi_\ell^{\mathrm{na,eq}}(\boldsymbol{r})$ on Π^ℓ, we now define $\psi^{\mathrm{na,eq}}$ on $\Pi=\cup_\ell\Pi^\ell=\{\text{faces of all } c_i\}$ to equal $\psi_\ell^{\mathrm{na,eq}}(\boldsymbol{r})$ for $\boldsymbol{r}\in\Pi^\ell$, and we proceed to the final portion of our algorithm.

(*c*) *Evaluation of the surface values of* $\psi_\ell^{\mathrm{na,eq}}$

The field $\psi^{\mathrm{na,eq}}(\boldsymbol{r})$, which has thus far been obtained for $\boldsymbol{r}\in\Pi$, is a high-order approximation of the corresponding field induced at any point in $\boldsymbol{r}\in\Pi$ by the set of all true sources which are not adjacent to $\boldsymbol{r}$. Thus, by solving a Dirichlet problem with boundary values $\psi^{\mathrm{na,eq}}(\boldsymbol{r})$ in each cell c_i, the full non-adjacent field can be obtained at every surface discretization point. This Dirichlet problem can be solved uniquely and in a stable manner since the size of the cells has been chosen so that internal resonances do not occur; see Bruno & Kunyansky (2001*a*) and Kunyansky & Bruno (2001) for a detailed error analysis in these regards.

In order to approximate the non-adjacent field inside a given cell, we use the discretized plane wave expansion (Felsen & Marcuvit 1973)

$$u(\boldsymbol{r})\approx\sum_{j=1}^{n^{\mathrm{wave}}}\zeta_j\exp(\mathrm{i}\boldsymbol{k}_j\boldsymbol{r}), \tag{5.4}$$

where $\boldsymbol{k}_j$ are unit vectors defining directions of wave propagation, and $\boldsymbol{\zeta}=(\zeta_1,\zeta_2,\ldots,\zeta_{n^{\mathrm{wave}}})$ is a vector of expansion coefficients. The procedure is quite similar to that

of § 5 *a*: the coefficients $\boldsymbol{\zeta}$ are found as a solution of an overdetermined system of equations which is obtained by matching the field values on $\partial\mathcal{S}_i$ with the plane wave expansion (5.4). As in § 5 *a*, by properly choosing the discretization directions we take advantage of the symmetries of the system and obtain eightfold complexity reductions. Finally, the plane wave expansions are evaluated at the surface discretization points, and the accelerated algorithm for evaluation of non-adjacent interactions is complete.

(*d*) *Solution of the discretized integral equation*

Sections 4 and 5 contain the main prescriptions for our fast and high-order integration scheme. Use of the iterative solver GMRES (Saad & Schultz 1986) (un-restarted) then gives rise to our fast high-order scattering solver. The number of iterations required to achieve convergence to a given accuracy is significantly affected by the value chosen for the parameter γ of equation (2.2). In our computations we use the value $\gamma = \max\{3, A/\lambda\}$, where A is the diameter of the scatterer. Indeed, our experiments have shown that this value of γ leads to a substantially reduced numbers of GMRES iterations—of the order of 10 to 20 iterations, even for acoustically large problems.

(*e*) *Overall complexity*

A detailed operation count for our algorithm is given in Bruno & Kunyansky (2001*a*); there it is shown that the overall complexity of our method is of order $\mathcal{O}(N^{6/5}\log N)$ to $\mathcal{O}(N^{4/3}\log N)$ operations—depending on the geometric characteristics of the scattering surface. In this section we describe the basic rationale behind our reduced complexity counts, which contrast with the $\mathcal{O}(N^{3/2}\log N)$ complexity of the classical FFT approaches (Bleszynski *et al.* 1996; Bojarski 1982; Catedra *et al.* 1989; Phillips & White 1997). Also, in table 1 we demonstrate numerically the $\mathcal{O}(N^{4/3}\log N)$ scaling of our algorithm for smooth surfaces.

As mentioned in the introduction and discussed in § 5 *a*, our algorithm subdivides the volume occupied by the scatterer into a number of (relatively large) cubic cells, and it places equivalent sources *on the faces* of those cells; see figure 2. This procedure is actually repeated three times, to obtain field values on all cell faces without resorting to a full volume FFT. Thus, in each one of the three field computations, the planes containing equivalent sources are separated by a distance H, which may be chosen to depend on N rather arbitrarily: $H = H(N)$. By using $H(N) \gg \mathcal{O}(N^{-1/2})$ one can obtain FFTs of size $\ll (N^{1/2})^3 = N^{3/2}$. Much increased values of $H(N)$, on the other hand, give rise to correspondingly increased costs for the evaluation of the adjacent interactions and calculation of equivalent source intensities. The optimization calculations given in Bruno & Kunyansky (2001*a*) show that the optimal choice of $H(N)$ leads to the operation counts quoted above for our algorithm. The $\mathcal{O}(N^{4/3}\log N)$ estimate applies to smooth surfaces, for which our high-order algorithm provides accurate solutions with small values of N; the more favourable $\mathcal{O}(N^{6/5}\log N)$ count is valid for highly complex surfaces requiring significant amounts of subwavelength sampling.

(This difference in operation counts arises as highly complex surfaces require discretizations which can be significantly finer than those required to resolve the acoustic wavelength alone. Thus, the exponent β determining the size $\mathcal{O}(N^{\beta})$ of the required

Table 1. *Complexity scaling study for the various portions of the algorithm*

	small ellipsoid	large ellipsoid	ratio
size (in wavelengths λ)	$28.6 \times 7.2 \times 7.2$	$80 \times 20 \times 20$	$\approx \sqrt{8}$
number of unknowns	86 878	691 206	≈ 8
maximum error	2.6×10^{-4}	1.4×10^{-4}	0.54
time required for ...			
... construction of interpolating splines (§ 4)	28 s	260 s	9.3
... evaluation of adjacent interactions (§ 4)	1242 s	16 241 s	13.1
... decomposition of matrices of §§ 5 *a*, *c*	1 s	2 s	2
... evaluation of equivalent source intensities	93 s	1061 s	11.4
... computation of convolutions in (5.3)	46 s	145 s	3.2
... subtraction of adjacent FFTs (§ 5 *b*)	243 s	1642 s	6.8
... evaluation of surface values (§ 5 *c*)	15 s	119 s	7.9
total time per iteration	1640 s	19 469 s	11.9

FFTs, which for a given interplane spacing and a given prescribed accuracy depends on the wavelength only, can be substantially smaller for complex surfaces ($\beta = 6/5$) than for smooth surfaces ($\beta = 4/3$); see Bruno & Kunyansky (2001*a*) for details.)

Table 1 displays computing times used by the various portions of our algorithm in problems of scattering by two ellipsoids with equal aspect ratios: (4:1:1). The ratio of acoustical sizes for these ellipsoids is $\sqrt{8}$. Correspondingly, the number of unknowns used for the larger ellipsoid was chosen to equal $\sqrt{8}^2 = 8$ times that used for the smaller ellipsoid. We see that the accuracy does not deteriorate with the increased problem size. Further, the overall increase in computing time is in fact smaller than our estimated factor of $8^{4/3} = 16$; we expect the asymptotic full $\mathcal{O}(N^{4/3} \log N)$ behaviour would be observed for considerably larger problems.

6. Numerical results

We first compare results provided by our *non-accelerated* high-order scattering solver with corresponding results given by the high-order methods of Canino *et al.* (1998). (Here and in what follows we used the value $\eta = \max\{3, d/\lambda\}$ for the coupling constant η of equation (2.2), where d is the diameter of the scatterer. Indeed, we have found that this value of η leads to a reduced number of GMRES iterations.) In table 2 we thus present computations of scattering by a sphere of radius 2.7λ. In the computing time portion of table 2, we only show *the set-up time reported in* Canino *et al.* (1998), since in that work a slow LU decomposition was used to solve the resulting linear system. In the entries corresponding to our algorithm we show the full time required for the solution of the boundary integral equation. The notation NA in our tables indicates results obtained by means of the non-accelerated version of our algorithm.

In examining the time portions of table 2, it should be borne in mind that different computers were used (a Sparc 10 in Canino *et al.* (1998) and a 400 MHz PC in our work) and different problems were solved (a Maxwell system in Canino *et al.* (1998)

Table 2. *Performance of three high-order methods: the high-order Nyström and Galerkin techniques of Canino et al. (1998) and the present algorithm*

algorithm	radius	time	unknowns	RMS error
Nyström (Canino *et al.* 1998)	2.7λ	1 953 s (set-up)	5400	2.3%
Galerkin (Canino *et al.* 1998)	2.7λ	38 803 s (set-up)	5400	0.48%
present (NA)	2.7λ	294 s	2526	0.068%
present (NA)	2.7λ	1430 s	5430	0.0025%

Table 3. *Scattering by spheres of radii* 12λ *and* 24λ *as computed by FISC and the present algorithm*

algorithm	radius	time	RAM	unknowns	RMS error	computer
FISC	12λ	12 h	1.8 Gb	602 112	7.2%	SGI Power Challenge R8000
present (NA)	12λ	6.5 h	24 Mb	26 214	0.22%	Pentium II 400 MHz
present	12λ	16 h	120 Mb	87 318	0.000 96%	Pentium II 400 MHz
FISC	24λ	8×5 h	5 Gb	2 408 448	7.9%	SGI Origin 2000 (8 processors)
present	24λ	$33h$	807 Mb	349 830	0.024%	Pentium II 400 MHz

Table 4. *Scattering from large ellipsoids; point source inside the body*

type	(ka, kb, kc)	#it	time/it	RAM	unknowns	max. error	RMS error
accelerated	(150,37.5,37.5)	18	112 min	490 Mb	298 806	3.7×10^{-4}	8.8×10^{-6}
accelerated	(200,50,50)	18	112 min	490 Mb	298 806	1.3×10^{-3}	2.2×10^{-5}

and the Helmholtz equation in our work). It should also be emphasized that, as mentioned above, only the set-up time of the high-order integrator of Canino *et al.* (1998) is shown. We see that our method produces substantially more accurate results than those of Canino *et al.* (1998), in computing times which are comparable or smaller than the set-up portions reported in that work.

Table 3 compares the performance of our accelerated algorithms with that of FISC (Song *et al.* 1988) in the computations of scattering from large spheres. We see that the present algorithm achieves considerably higher accuracy than Song *et al.* (1988) with lesser or comparable computational resources. The efficiency of our algorithm results, in part, from the fact that a lower discretization density suffices for our integrator to yield highly accurate results.

Table 4 shows accuracies and computation times for scattering from large ellipsoids with radii (a, b, c). The results presented in tables 3 and 4 can be compared with the large-scale computations of Bleszynski *et al.* (1996). In the latter work the adaptive integral method running on 40 IBM SP2 nodes was used to compute

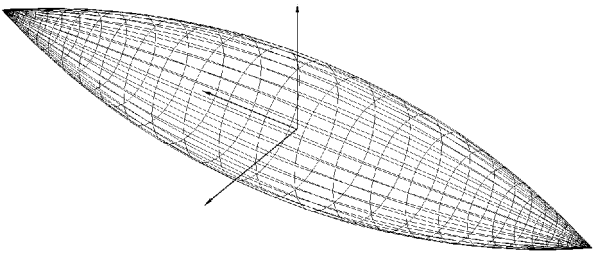

Figure 3. Ogive.

Table 5. *Scattering by a one-wavelength long ogive. Non-accelerated computations*

grid	unknowns	iterations	time/it	maximum error
49×32	1 568	20	69 s	2.5×10^{-3}
99×64	6 336	17	12 min 45 s	3.8×10^{-5}
199×128	25 472	17	3 h 27 min	9.8×10^{-7}

(electromagnetic) scattering from the bodies up to the size $70\lambda \times 40\lambda \times 15\lambda$ (or $(ka, kb, kc) = (220, 126, 47)$); no error estimates were provided in that work.

Finally, we present preliminary results obtained for the scattering from surfaces with singularities. Table 5 shows the accuracy obtained from our methods in the solution of a scattering problem for a one-wavelength-long ogive depicted in figure 3. This test body was described in Woo *et al.* (1993).

Here, to facilitate error evaluation, we used boundary conditions as given by a unit source located inside the ogive—for which the exact solution is the field of the source itself. Our 'analytic' method to resolve a geometric singularity is akin to the one we use for resolution of the Green function singularity: namely, a change to an appropriately chosen polar coordinate system provides a preliminary regularization. Use of polynomial changes of variables around each singular point, be it a point or line singularity, then provides the needed additional regularization; see Bruno & Kunyansky (2001*b*).

Effort sponsored by the Air Force Office of Scientific Research, Air Force Materials Command, USAF, under grant numbers F49620-96-1-0008, F49620-99-1-0010. O.P.B. gratefully acknowledges support from NSF (through an NYI award and through contracts DMS-9523292 and DMS-9816802), and from the Powell Research Foundation. The US Government is authorized to reproduce and distribute reprints for governmental purposes notwithstanding any copyright notation thereon. The views and conclusions contained herein are those of the authors and should not be interpreted as necessarily representing the official policies or endorsements, either expressed or implied, of the Air Force Office of Scientific Research or the US Government.

References

Bleszynski, E., Bleszynski, M. & Jaroszewicz, T. 1996 AIM: adaptive integral method for solving large-scale electromagnetic scattering and radiation problems. *Radio Sci.* **31**, 1225–1251.

Bojarski, N. 1982 The k-space formulation of the scattering problem in the time domain. *J. Acoust. Soc. Am.* **72**, 570–584.

Bruno, O. P. & Kunyansky, L. 2001*a* A fast, high-order algorithm for the solution of surface scattering problems: basic implementation, tests and applications. *J. Computat. Phys.* **169**, 80–110.

Bruno, O. P. & Kunyansky, L. 2001*b* High-order solution of wave scattering problems: corners, edges and other geometric singularities. (In preparation.)

Canino, L., Ottusch, J., Stalzer, M., Visher, J. & Wandzura, S. 1998 Numerical solution of the Helmholtz equation using a high-order Nyström discretization. *J. Computat. Phys.* **146**, 627–663.

Catedra, M. F., Cago, E. & Nuno, L. 1989 A numerical scheme to obtain the RCS of three-dimensional bodies of resonant size using the conjugate gradient method and the fast Fourier transform. *IEEE Trans. Antennas Propagat.* **37**, 528–537.

Coifman, R., Rokhlin, V. & Wandzura, S. 1993 The fast multipole method for the wave equation: a pedestrian prescription. *IEEE Antennas Propagat. Mag.* **35**, 7–12.

Colton, D. & Kress, R. 1992 *Inverse acoustic and electromagnetic scattering theory*. Springer.

Dembart, B. & Yip, E. 1998 The accuracy of fast multipole methods for Maxwell's equations. *IEEE Computat. Sci. Engng* **5**(3), 48–56.

Duffy, M. G. 1982 Quadrature over a pyramid or cube of integrands with a singularity at a vertex. *SIAM J. Numer. Analysis* **19**, 1260–1262.

Felsen, L. B. & Marcuvitz, N. 1973 *Radiation and scattering of waves*. Englewood Cliffs, NJ: Prentice-Hall.

Golub, G. H. & Van Loan, C. F. 1989 *Matrix computations*, 2nd edn. Johns Hopkins University Press.

Greengard, L., Huang, J. F., Rokhlin, V. & Wandzura, S., 1998 Accelerating fast multipole methods for the Helmholtz equation at low frequencies. *IEEE Comput. Sci. Engng* **5**, 32–38.

Kunyansky, L. & Bruno, O. P. 2001 A fast, high-order algorithm for the solution of surface scattering problems. II. Theoretical considerations. (Submitted.)

Labreuche, C. 1998 A convergence theorem for the fast multipole method for 2-dimensional scattering problems. *Math. Computat.* **67**, 553–591.

Phillips, J. R. & White, J. K. 1997 A precorrected-FFT method for electrostatic analysis of complicated 3D structures. *IEEE Trans. CAD Integr. Circuits Syst.* **16**, 1059–1072.

Rokhlin, V. 1990 Rapid solution of integral equations of scattering theory in two dimensions. *J. Computat. Phys.* **86**, 414–439.

Rokhlin, V. 1993 Diagonal form of translation operators for the Helmholtz equation in three dimensions. *Appl. Computat. Harmon. Analysis* **1**, 82–93.

Saad, Y. & Schultz, M. H. 1986 GMRES: a generalized minimal residual algorithm for solving non-symmetric linear systems. *SIAM J. Sci. Comput.* **7**, 856–869.

Song, J. M., Lu, C. C., Chew, W. C. & Lee, S. W. 1988 Fast Illinoic Solver Code (FISC). *IEEE Antennas Propagat. Mag.* **40**, 27–34.

Song, J. M., Lu, C. C. & Chew, W. C. 1997 Multilevel fast multipole algorithm for electromagnetic scattering by large complex objects. *IEEE Trans. Antennas Propagat.* **45**, 1488–1493.

Woo, A. C., Wang, H. T. G., Schuh, M. J. & Sanders, M. L. 1993 Benchmark radar targets for the validation of computational electromagnetics programs. *IEEE Antennas Propagat. Mag.* **35**, 84–89.